Proceedings of the 6th European VLBI Network Symposium
Ros, E., Porcas, R.W., Lobanov, A.P., & Zensus, J.A. (eds.)
June 25th-28th 2002, Bonn, Germany

Internal structure of compact relativistic jets

A. P. Lobanov and J. A. Zensus

Max-Planck-Institut für Radioastronomie, Auf dem Hügel 69, Bonn 53121, Germany

Abstract. We present first direct evidence for the presence of plasma instability in an extragalactic relativistic jet, based on analysis of VSOP observation of the quasar 3C273 made at 5GHz. In the VSOP image of 3C273, the emission across the jet is resolved, revealing two threadlike patterns that form a double helix inside the jet. We have identified 5 wavelengths contributing to the appearance of the patterns inside the jet. These wavelengths are in good agreement with the predicted wavelengths of several modes of Kelvin–Helmholtz (K–H) instability developing in a light jet with Lorentz factor of 2 and Mach number of 3.5. The K–H instability description reproduces in detail the internal structure of the jet on scales of up 300 parsecs.

1. Introduction

One of the most intriguing features observed in AGN are highly collimated, relativistic plasma outflows (jets) which originate in the vicinity of the center of activity and propagate at distances of up to several megaparsecs. Finding direct evidence for plasma instability in extragalactic jets is crucial for understanding the nature of relativistic outflows from active galactic nuclei (AGN). Our recent radio interferometric observations of the quasar 3C273 made with VSOP[1] (Hirabayashi et al. 1998) have yielded an image in which the emission across the jet is resolved, revealing two thread–like patterns which form a double helix inside the jet. The quasar 3C273 is one of the closest, most luminous, and best studied AGN, with a prominent jet observed in the X–ray, optical and radio wavebands. The jet in 3C273 is one–sided, with no signs of emission on the counter–jet side at dynamic ranges of up to 16,000:1 (Unwin et al. 1985). The enhanced emission features (jet components) identified in the jet on scales of up to ∼20 milliarcseconds (mas) are moving at apparent speeds exceeding the speed of light by factors of 5–8 (Abraham et al. 1996). The structure and kinematics of such outflows are typically explained in terms of shocks and Kelvin–Helmholtz instability developing in a relativistic plasma. Recent studies (Hardee 2000) have shown that the instability may produce complex, three–dimensional ribbon–like and thread–like patterns inside a relativistic jet. In these ribbons and threads, a substantial increase of particle pressure and radio emissivity can be expected. For relatively close AGN like 3C273, the resolution of Space VLBI observations is sufficient for resolving the internal structure of their jets. We present here the analysis of a VSOP image of radio emission at $\lambda = 6$ cm from the parsec–scale jet in 3C273 (Lobanov et al. 2000), and show that it can be explained by a combination of several modes of Kelvin–Helmholtz instability developing in the jet plasma.

[1] VLBI Space Observatory Programme

2. The interior of the jet in 3C273

We reproduce the VSOP image and four emission profiles measured across the jet in Figure 1. The image reveals a remarkable internal structure of the jet, benefiting from the favorable orientations of the space baselines which provide a 0.7–mas resolution in the direction perpendicular to the jet axis. At the redshift of 3C273 ($z = 0.158$, Strauss et al. 1992), this corresponds to a linear scale of 1.7 pc (for $q_0 = 0.5$ and $H_0 = 70$ km s^{-1}Mpc^{-1}). The complexity of the emission distribution across the jet is particularly visible in the profiles shown in the inset of Figure 1. Extensive tests of the reliability of the VSOP image yield the most conservative limit on the dynamic range of the image of about 700:1 (Lobanov & Zensus 2001), which is sufficient for the purposes of studying the emission distribution along, and across, the jet. To determine the interior structure of the jet, we have obtained 240 profiles of brightness distribution across the jet. All of the profiles are centered on the smoothed ridge line of the jet (shown by the dashed line in Figure 1). Each profile is oriented orthogonally to the local direction of the ridge line. The centers of adjacent profiles are separated by 0.1 mas, which provides a sufficient redundancy of the measurements. In most of the profiles, at least two distinct features are visible. We fit each profile by two Gaussians (Gaussian components) and determine their positions, amplitudes and widths. We designate the two Gaussian components as P1 and P2, and plot the locations of their peaks in Figure 1. The two components fitted can be easily distinguished by their size and strength, with the component P1 being typically stronger and more compact than P2 (Figure 2).

The threads P1 and P2 plotted in Figure 1 form a regular pattern, resembling a double helix. The presence of such a pattern is a compelling sign of Kelvin–Helmholtz (K–H) instability developing in an outflow which has transverse velocity gradients or discontinuities due to interaction between the flowing relativistic plasma and (typically) sub–relativistic surrounding material.

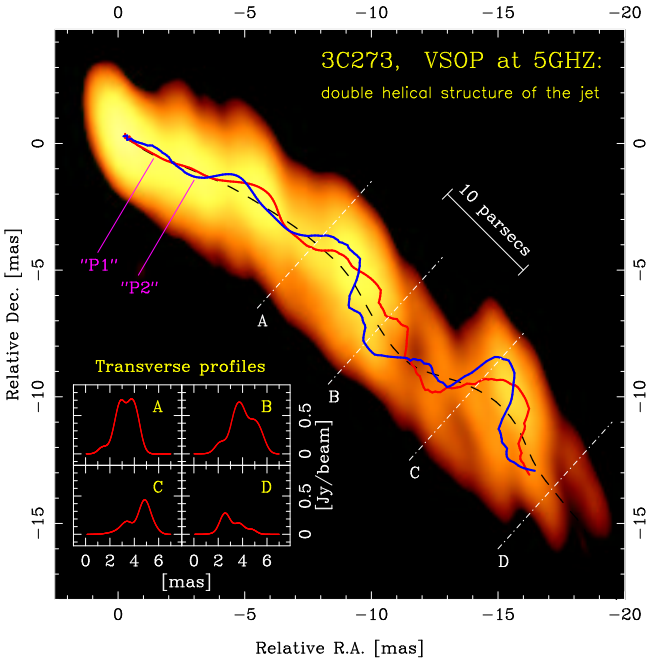

Fig. 1. Parsec–scale radio jet in 3C273 imaged at 5 GHz by the VSOP. The VSOP image has a restoring beam of 2.09×0.70 mas at P.A.= 12.9°; the peak flux density in the image is 4.52 Jy/beam. The dot-dashed white lines denote the locations of the 4 flux density profiles shown in the inset. The locations of the two thread–like features, P1 and P2, identified in the jet are marked in the image by the red and blue lines.

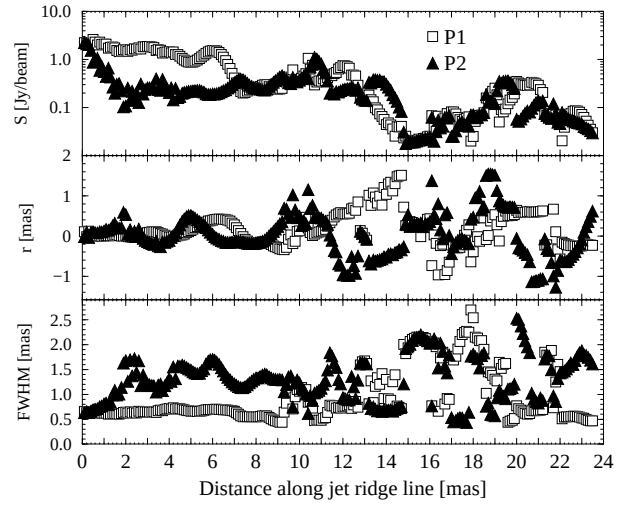

Fig. 2. Amplitudes (top), position offsets (middle) and widths (bottom) of the two Gaussian components fitted to the transverse profiles of the jet in 3C273.

3. Modeling the position offsets of P1 and P2

To connect the measured properties of the jet in 3C273 with theoretical models describing K–H instability, we first approximate the position offsets of the threads P1 and P2 by a sum of several sinusoidal modes, and determine their wavelengths, phases, and amplitudes. Each individual sinusoidal mode, r_i, is described by a set of four parameters: wavelength λ_i, phase ψ_i, maximum amplitude a_i, and distance z_i at which the maximum amplitude is reached. The evolution of a mode is described by an amplitude term $\mathcal{G}_i(z) = a_i\,(2\,z\,\mathrm{e}^{1-z/z_i})/(z+z_i)$, where z is the coordinate along the jet axis. The corresponding position offset introduced by the mode in the picture plane is $r_i(z) = \mathcal{G}_i(z)\cos[\psi_i + 2\pi z(\lambda_i(1+z\sin\phi_\mathrm{j}))^{-1}]$, where ϕ_j describes the half–opening angle of the jet.

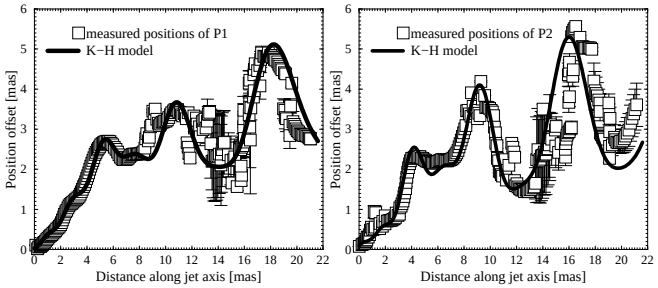

Fig. 3. The positions of P1 and P2 fitted by a model of Kelvin–Helmholtz instabilities propagating in the jet. The parameters of the contributing instability modes are listed in Table 1.

We find that five of such modes are required to represent the positions of P1 and P2. The fits obtained are shown in Figure 3, and the parameters of the modes are given in the columns 1–5 of Table 1. The first two fitted modes of P1 are identical to the respective modes of P2. The modes 4 and 5 of P1 differ only in their phases from the respective modes of P2. The offset between the respective phases of the 3-rd, 4-th, and 5-th modes of P1 and P2 is 180°. In addition to that, the 3-rd and 4-th modes in each thread are also offset by 180° from each other. Preserving these phase offsets is a crucial requirement: changing any of them by as little as 5° results in a dramatic deterioration of the fit. Another critical condition is the closeness of the wavelengths of the 3-rd and 4-th modes in both threads. No good fit can be achieved whenever the relative ratio of these wavelengths is increased even by only 10%. This also implies that the 3-rd and 4-th modes must not interfere destructively with each other. The relationships between different modes described above reduce the effective number of the fitting free parameters to 16, providing an additional assurance that the fits obtained are not overdetermined. We conclude therefore that P1 and P2 are produced by essentially the same set of 5 sinusoidal modes. The observed relations between the fitted parameters of these modes are then readily explained in the framework of K–H instability. The first and second fitted modes are likely to represent two different surface instability modes (since the surface modes should have the same effect on both threads). The other three fitted modes should correspond to the body modes of the instability (thus producing two threads inside the jet propagating with a 180° phase offset between them).

It has been shown (Hardee 2000) that a long wavelength helical surface mode ($\mathrm{H}^\mathrm{l}_\mathrm{s}$, similar to the resonant helical surface mode $\mathrm{H}^\star_\mathrm{s}$ and a resonant helical first body mode ($\mathrm{H}^\star_\mathrm{b1}$) are likely to produce ribbon–like structures

inside a relativistic jet. The presence of an elliptical normal mode (most likely, a combination of elliptical surface and body modes) may produce double threads intertwining around each other, whenever the emission is coming from the interior density and pressure enhancements. The correspondence between the fitted modes and the modes of Kelvin–Helmholtz instability can be established quantitatively by calculating the characteristic wavelength, $\lambda^\star = \lambda_i(n_i + 2m_i + 1/2)$, where n_i and m_i are the azimuthal wavenumbers of the instability mode identified with the measured wavelength λ_i. The characteristic wavelength depends only on the physical conditions in the jet, and therefore it must be the same in all of the fitted modes for which a K–H instability mode has been correctly identified. We find that the fitted modes admit only one physically plausible combination of K–H instability modes. This combination is described in columns 6–8 of Table 1. According to Table 1, the modes 2–5 must grow at their resonant wavelengths, with the corresponding average $\lambda^\star_{[2-5]} = 14.5 \pm 3.1$. The much larger $\lambda^\star$ of the first mode indicates that the helical surface mode must be driven externally. The driving mechanism for the $\mathrm{H_s}$ mode can be associated with the 15–year period suggested from the observed changes of the ejection angle in the jet of 3C273 (Abraham & Romero 1999).

4. Physical model for the jet in 3C273

The spatial and temporal evolution of different modes of K–H instability depend ultimately on the plasma speeds and Mach numbers in the flow itself (β_j, M_j) and in the surrounding medium (β_x, M_x), as well as on the ratio, $\eta = \rho_\mathrm{j}/\rho_\mathrm{x}$, between the densities in the flow and the surrounding medium. For the purpose of applying the perturbation analysis, it is sufficient to assume that the jet has a conical shape with the radius R_j measured at the jet origin and a small opening half–angle $\phi_\mathrm{j} \ll 1/M_\mathrm{j}$ (ensuring that the evolution of K–H instability is well approximated by the solutions obtained for a cylindrical jet; Hardee 1986,1987,2000). The jet flow is directed at an angle θ_j with respect to the line of sight, and the jet plasma moves at a speed characterized by a Lorentz factor $\Gamma_\mathrm{j} = (1 - \beta_\mathrm{j}^2/c^2)^{-1/2}$. These assumptions are sufficient for estimating the resonant and longest unstable wavelengths of different modes of K–H instability (taking into account the propagation speed, v_w, of the instability). An additional constraint is given by the driving period $P_\mathrm{o} = 15$ years which we associate with the $\mathrm{H_s}$ mode. The left panel of Table 2 lists physical parameters of the jet which provide the best description of the measured wavelengths and satisfy the observed P_o. The errors of the model parameters are 1σ–deviations determined from χ^2 parameter of the fit. These errors are used for calculating the respective errors of the derived jet properties and mode wavelengths.

The right panel of Table 2 compares the predicted and measured wavelengths of individual instability modes. For all of the identified instability modes (shown in bold in Table 2), the predicted and measured wavelengths agree within the formal errors of the model. The model also provides a self–consistent explanation for the correlations found in the fitted modes identified with the surface modes, helical body modes, and elliptical body modes. We would like to emphasize that the jet description outlined in Table 2 explains in detail the internal structure of the jet on scales $\gtrsim 30$ mas ($\gtrsim 300$ pc), accommodates the general morphology of the jet on scales of $\gtrsim 100$ mas ($\gtrsim 1$ kpc), and accounts for the observed periodic changes of the jet ejection angle. The model also provides a better understanding of the physical nature of different instability modes:

4.1. Surface modes

The model gives an exceptionally good agreement for the two longer modes: $\mathrm{H_s}$, $\mathrm{E^\star_s}$. These modes ($\mathrm{H_s}$ and $\mathrm{E^\star_s}$) are the surface modes of K–H instability which cause displacements and distortions of the entire jet, and therefore they would manifest themselves in exactly the same way in P1 and P2. For the jet parameters given in Table 2, the expected ratio between the growth lengths (z_i) of the surface and body modes used in the model is 1.8–2.6 (the measured ratio is 2.0, as seen from Table 1). This supports the identification of the two longer measured wavelengths with the surface modes of K–H instability.

4.2. Helical body modes

The wavelengths of the 3-rd measured mode identified with the $\mathrm{H^\star_{b1}}$ mode are different in P1 (3.9 mas) and P2 (4.1 mas). The $\mathrm{H^\star_{b1}}$ mode is a helical mode which has a single "arm" of enhanced density/pressure developing in the jet interior, and it is therefore asymmetric. Since the 3-rd mode must be in resonance with the 4-th mode, the emission enhancements produced by the 3-rd mode must be offset by 180° from each other, and their respective distances from the center of the jet cross–section must be different. The stronger and more compact enhancement (P1) should then be located closer to the center, and grow at a slightly shorter wavelength. The $\mathrm{H_{b2}}$ mode cannot be identified with any of the measured wavelengths. It is possible that this (and perhaps all higher helical body modes) are blended with each other, or damped in the jet.

4.3. Elliptical body modes

Within the errors of the model, the $\mathrm{E^\star_{b1}}$ mode can be associated with the measured 3.8–mas wavelength. The shortest measured wavelength (1.9–mas) can be formally matched by the resonant wavelengths of three different instability modes ($\mathrm{H^\star_{b3}}$, $\mathrm{E^\star_{b2}}$, $\mathrm{E^\star_{b3}}$). We prefer to identify it with the $\mathrm{E_{b2}}$ mode, since this provides a more consistent physical picture. It is also possible that the 1.9–mas wavelength results from a combination of several short–wavelength modes. In either case, a combination of this

Table 1. Measured parameters of the modes contributing to P1 and P2

(1) Mode	(2) λ_i [mas]		(3) a_i [mas]		(4) ψ_i [deg]		(5) z_i [mas]		(6) K–H mode	(7) ϵ_{λ_i}	(8) $\lambda^\star$ [mas]
	P1	P2	P1	P2	P1	P2	P1	P2	P1,2	P1,2	P1,2
1	18.0		1.5		180		40		H_s		27.0
2	12.0		1.4		260		40		$E_s^\star$	7%	15.0
3	3.9	4.1	2.2	1.5	315	135	20		$H_{b1}^\star$	4%	14.4
4	3.8		1.2		135	315	20		$E_{b1}^\star$	15%	16.0
5	1.9		0.25		175	355	20		$E_{b2}^\star$	10%	12.4

Columns of the table represent: 1 – mode number; $2, 3, 4, 5$ – fitted wavelength, amplitude, phase, and peak distance; 6 – K-H mode identified with the fitted wavelength; 7 – discrepancy between the measured and theoretical wavelength of the corresponding K-H mode; 8 – characteristic wavelength.

Table 2. Kelvin–Helmholtz instability model for the jet in 3C273

Model parameters			Model predictions			Measurements	
Lorentz factor,	Γ_j	2.1 ± 0.4	Mode[a)]	$\lambda^\star_{n,m}$ [mas]	$\lambda^1_{n,m}$ [mas]	λ_i [mas]	Identification
Mach number,	M_j	3.5 ± 1.4					
Density ratio,	η	0.023 ± 0.012	$\mathbf{H_s}$	9.8 ± 2.3	$\mathbf{18.0 \pm 4.6}$[b)]	**18.0**	positive[b)]
Jet radius [pc],	R_j	0.8 ± 0.2	$\mathbf{H_{b1}}$	$\mathbf{4.2 \pm 1.0}$	7.7 ± 1.9	**3.9-4.1**	positive
Jet half–opening angle,	ϕ_j,	$1.5^\circ \pm 0.2^\circ$	H_{b2}	2.7 ± 0.6	4.3 ± 1.0	...	damped?
Jet viewing angle,	θ_j	$15^\circ \pm 3^\circ$	H_{b3}	1.9 ± 0.5	2.9 ± 0.7	1.9[c)]	probable
Calculated jet properties			$\mathbf{E_s}$	$\mathbf{11.9 \pm 2.8}$	—	**12.0**	positive
Jet sound speed,	a_j	0.53 ± 0.16	$\mathbf{E_{b1}}$	$\mathbf{3.3 \pm 0.8}$	5.5 ± 1.3	**3.8**	positive
Ambient medium sound speed,	a_x	0.08 ± 0.03	$\mathbf{E_{b2}}$	$\mathbf{2.3 \pm 0.5}$	3.5 ± 0.8	**1.9**[c)]	positive
Instability propagation speed,	v_w	0.21 ± 0.06	E_{b3}	1.7 ± 0.4	2.6 ± 0.6	1.9[c)]	probable

Notes: *a)* – bold face marks modes most likely present in the jet; *b)* – externally driven mode; *c)* – possible multiple modes acting together.

mode with the other two body modes identified in the jet would produce internal pressure and density enhancements forming a double–thread structure inside the jet, with the individual threads offset from each other by 180°.

5. Conclusions

The VSOP observation of the parsec–scale structures in the quasar 3C273 has enabled establishing the presence, and determining the properties, of Kelvin–Helmholtz instability in a relativistic, extragalactic jet. An important conclusion from the model parameters obtained is that the instability is developing in a plasma with moderate Lorentz factor and Mach number and a much lower density than that of the surrounding material. The calculated sound speeds agree well with the values expected for a light, electron–positron jet plasma and a sub–relativistic ambient medium. The derived $\Gamma_j = 2.1$ corresponds to an apparent speed $\beta_{app} = \beta_j \sin\theta_j/(1 - \beta_j \cos\theta_j) = 1.4c$, which is lower than the apparent speeds of 5–8c typically measured in the jet of 3C273 (Abraham et al. 1996). However, the apparent speeds are determined from the motions of enhanced emission features most likely associated with relativistic shocks inside the jet. The bulk Lorentz factor of these features can be much higher than the Lorentz factor of the underlying flow. In contrast to this, the speed inferred from fitting the positions of the threads P1 and P2 reflects the speed of the slower, underlying flow in which the instability develops. This implies that there should be a substantial velocity gradient across the jet.

References

Abraham, Z., Carrara, E., Zensus, J.A., Unwin, S.C. 1996, A&AS, 115, 543.

Abraham, Z. & Romero, G.E. 1999, A&A, 344, 61.

Hardee, P.E. 1986, ApJ, 303, 111.

Hardee, P.E. 1987, ApJ, 313, 607.

Hardee, P.E. 2000, ApJ, 533, 176.

Hirabayashi, H., Hirosawa, H., Kobayashi, H., et al. 1998, Science, 281, 1825.

Lobanov, A.P., Zensus, J.A., Abraham, Z., et al. 2000, Advances in Space Research, 26, 669.

Lobanov, A.P., Zensus, J.A. 2001, Science, 294, 128.

Strauss, M.A., Huchra, J.P., Davis, M., et al. 1992, ApJS, 83, 29.

Unwin, S.C., Cohen, M.H., Biretta, J.A., et al. 1985, ApJ, 280, 109.